# A WH/GSMT-Based Full-Wave Analysis for Planar Transmission Lines Embedded in Multilayered Dielectric Substrates

Ling-Miao Chou, Roberto G. Rojas, *Senior Member, IEEE,* and Prabhakar H. Pathak, *Fellow, IEEE,*

***Abstract*—A new full-wave analysis method, referred to as the WH/GSMT, is developed to solve multilayered planar transmission line problems. First, the scattering of an obliquely incident parallel plate mode (PPM) by a PEC half plane embedded in a multilayered isotropic dielectric substrate within a PEC parallel plate region is analyzed via the Wiener-Hopf (WH) technique. The solution is then incorporated into the generalized scattering matrix technique (GSMT) to find the (complex) propagation constant and characteristic impedance of the planar transmission lines. The lateral power leakage is taken into account rigorously in the WH/GSMT. Numerical results including the microstrip line, conductor-backed slotline, coupled microstrip lines, and antipodal finlines are presented along with a discussion of the advantages/disadvantages of this method.**

## I. Introduction

A NEW rigorous full-wave analysis method, referred to as the WH/GSMT, is presented to solve multilayered planar transmission line problems [1], [2]. The planar transmission lines considered here are assumed to be perfect electric conductors (PEC) of infinitesimal thickness which are embedded in multilayered isotropic dielectric substrates. The WH/GSMT consists of two key steps. First, the canonical scattering problem of an obliquely incident PPM by the edge of a PEC half plane embedded in a multilayered dielectric substrate within a PEC parallel plate region, as depicted in Fig. 1, is analyzed via the WH technique. Fig. 2 shows the side view of the geometry. Note that a PEC top cover is included in order to simplify the factorization process in the WH procedure, which otherwise involves a complicated integral due to the branch cut in the corresponding open region problem. However, as long as the circuit is used for guided waves rather than radiation, the effect of the top cover is negligible if placed far enough. The solution is then written in the form of compact scattering matrices and incorporated in the GSMT formulation [3], [4] to solve planar transmission line problems. The whole scheme can be viewed as an important extension of Oliner and Lee's work [6], [7] or a more efficient version of the mode matching method [3]. Note that in the mode matching method, the coefficients of the scattering matrices for the canonical half plane problem are obtained numerically, whereas, they are obtained analytically in the WH/GSMT.

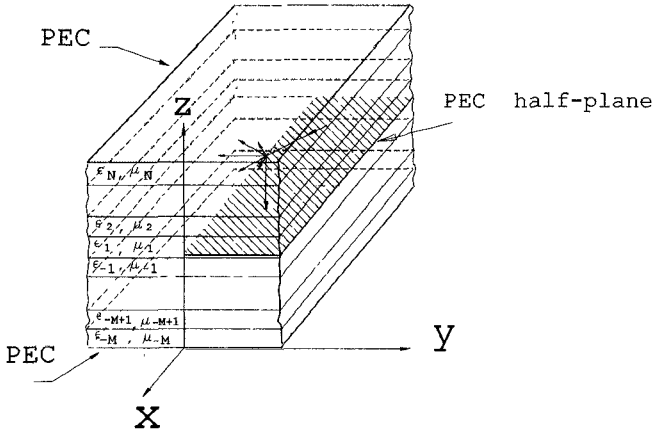


Fig. 1. The geometry of the canonical problem: A PEC half plane embedded in a multilayered dielectric region within a PEC parallel plate waveguide.

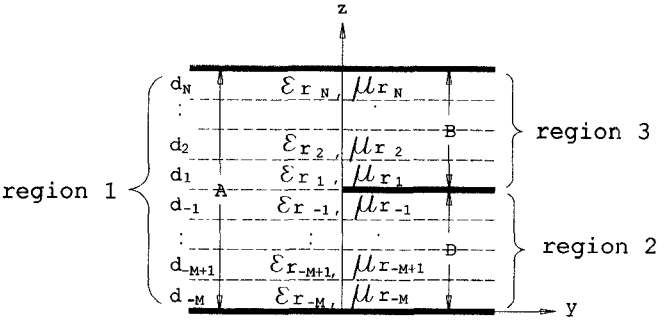


Fig 2. Side view of the geometry of the canonical problem depicted in Fig. 1.

Besides its crucial role in the WH/GSMT method, the canonical half plane scattering problem is by itself interesting and important in other applications. The WH procedure used here is a generalization of the work by Chang and Kuester [8], who considered the single-layered case, to treat the more complex multilayered geometry. Although the WH procedure is highly analytical, it can yield formally exact, closed-form solutions. The key steps of the WH analysis are presented here in a systematic way so that the solution to the multilayered case can be obtained by extending the solution to the single-layered geometry in a straightforward manner. It is also

Manuscript received February 1, 1993; revised March 21, 1994. This work was supported in part by the Joint Services Electronics Program (Contract N00014-89-J-1007) and by the Ohio State University Research Foundation.

The authors are with the Department of Electrical Engineering, ElectroScience Laboratory, Ohio State University, Columbus, Ohio 43212-1191 USA.

IEEE Log Number 9406804.

possible to observe some interesting analogies between the WH/GSMT and the spectral domain approach (SDA) [3], [9], [10], [13], such as the Green's function, basis functions, and so on. Moreover, although the SDA has been applied to solve planar transmission line problems for a long time [3], [9], [10], the lateral power leakage to source-free characteristic modes, like the surface wave modes, has not been taken into account rigorously until recently [11]. In the WH/GSMT, the lateral power leakage is contained in the analysis and no extra manipulation is needed when the propagation constant becomes complex.

This paper is organized as follows. The WH solution to the canonical half plane problem is presented in Section II. The transverse resonance relation for a single microstrip line built up with the GSMT is given in Section III. Numerical results based on the WH/GSMT for some common planar transmission lines, including the microstrip line, conductor-backed slotline, coupled microstrip lines, and antipodal finlines are given in Section IV. Coplanar waveguides with infinite/finite extent lateral ground planes have also been considered with this method; however, they will be discussed in another paper. Section V discusses the advantages/disadvantages of the WH/GSMT. The time convention $e^{j\omega t}$ is used and suppressed.

## II. WH Solution to the Half-Plane Problem

### A. Scattering of a $TM_z$ PPM Obliquely Incident from Region 2

Referring to Fig. 2, denote the region $y<0, 0<z<A$ as region 1; $y>0, 0<z<D$ as region 2; and $y>0, D<z<A$ as region 3. As is well known, the fields in the multilayered dielectric region are best expressed in terms of the $TE_z$ and $TM_z$ vector potentials. Assuming the incident field has the $e^{-jk_0\alpha x}$ dependence along the edge direction where $k_0$ is the free space wave number, then all the scattered fields must have the same dependence in the $x$ direction since the geometry is two dimensional. The common factor $e^{-jk_0\alpha x}$ will then be suppressed where $\alpha$ is a given constant for the canonical problem. We require $Re[\alpha]>0$ and $Im[\alpha] \leq 0$ in order to satisfy the radiation condition as $x \to \infty$. The Fourier transform of $f(y)$ is defined as usual by

$$\tilde{f}(\lambda) = \frac{k_0}{2\pi}\int_{-\infty}^{\infty} f(y)e^{jk_0\lambda y}\,dy = \tilde{f}_+(\lambda) + \tilde{f}_-(\lambda) \quad (1)$$

where $\tilde{f}_+(\lambda)$ and $\tilde{f}_-(\lambda)$ are the one-sided Fourier transforms, namely,

$$\tilde{f}_+(\lambda) = \frac{k_0}{2\pi}\int_{0}^{\infty} f(y)e^{jk_0\lambda y}\,dy \quad (2)$$

$$\tilde{f}_-(\lambda) = \frac{k_0}{2\pi}\int_{-\infty}^{0} f(y)e^{jk_0\lambda y}\,dy \quad (3)$$

The inverse Fourier transform is then given by

$$f(y) = \int_{-\infty}^{\infty} \tilde{f}(\lambda)e^{-jk_0\lambda y}\,d\lambda. \quad (4)$$

Before starting to solve the canonical scattering problem, some functions are first introduced such that the fields in each region can be easily described. As in the SDA [12], [13], the multilayered structure can be viewed as pieces of transmission lines connected together along the $z$ direction. Thus, the propagation matrices $\overline{\overline{P}}_e$ and $\overline{\overline{P}}_h$ for $TM_z$ and $TE_z$ polarized fields, respectively, are introduced. They are analogous to the ABCD matrix in microwave circuit theory, namely,

$$\overline{\overline{P}}_e(\lambda, z_j) = \begin{bmatrix} \cos(k_{z_j}z_j) & \frac{\epsilon_{r_j}}{k_{z_j}}\sin(k_{z_j}z_j) \\ -\frac{k_{z_j}}{\epsilon_{r_j}}\sin(k_{z_j}z_j) & \cos(k_{z_j}z_j) \end{bmatrix} \quad (5)$$

and

$$\overline{\overline{P}}_h(\lambda, z_j) = \begin{bmatrix} \cos(k_{z_j}z_j) & \frac{\mu_{r_j}}{k_{z_j}}\sin(k_{z_j}z_j) \\ -\frac{k_{z_j}}{\mu_{r_j}}\sin(k_{z_j}z_j) & \cos(k_{z_j}z_j) \end{bmatrix} \quad (6)$$

where $k_{z_j} = k_0\sqrt{\epsilon_{r_j}\mu_{r_j} - (\alpha^2+\lambda^2)}$ is the wave number along the $z$-axis in the $j$th layer, $\epsilon_{r_j}$ and $\mu_{r_j}$ are the corresponding relative permittivity and relative permeability, respectively, and $z_j$ is restricted to the range $-d_j \leq z_j \leq d_j$ along the $z$-axis. Note that $\overline{\overline{P}}_e$ and $\overline{\overline{P}}_h$ are defined in such a way that they are entire and even functions of $\lambda$. This property is very important since the WH analysis requires a rigorous knowledge of the analytical properties of the functions involved.

With the propagation matrices $\overline{\overline{P}}_e$ and $\overline{\overline{P}}_h$ defined above, one can then build up the functions $\psi_{de}$ and $\psi_{dh}$ (as well as $\psi_{be}$ and $\psi_{bh}$) along with their derivatives with respect to $z$ to express the $TM_z$ and $TE_z$-polarized fields in different regions. These functions incorporate the continuity condition between dielectric layers and the boundary condition at $z=D$ $(z=A)$ implicitly. Namely, in regions 1 and 2, the functions $\psi_{de}$ and $\psi_{dh}$ and their derivatives with respect to $z$ can be expressed as follows:

$$\left[\psi_{de}(\lambda, z), \frac{1}{\epsilon_{r_i}}\frac{\partial\psi_{de}(\lambda, z)}{\partial z}\right]^T = \overline{\overline{P}}_e(\lambda, z_i)\overline{\overline{P}}_e(\lambda, d_{i-1})\cdots\overline{\overline{P}}_e(\lambda, d_{-M})[1,0]^T \quad (7)$$

and

$$\left[\psi_{dh}(\lambda, z), \frac{1}{\mu_{r_i}}\frac{\partial\psi_{dh}(\lambda, z)}{\partial z}\right]^T = \overline{\overline{P}}_h(\lambda, z_i)\overline{\overline{P}}_h(\lambda, d_{i-1})\cdots\overline{\overline{P}}_h(\lambda, d_{-M})[0,1]^T \quad (8)$$

where $z_d = \Sigma_{j=-M, j\neq 0}^{i-1} d_j, z_i = z - z_d$, and $z$ is located in the $i$th layer of the dielectric substrate; whereas, in region 3, the functions $\psi_{be}$ and $\psi_{bh}$ and their derivatives are given by

$$\left[\psi_{be}(\lambda, z), \frac{1}{\epsilon_{r_i}}\frac{\partial\psi_{be}(\lambda, z)}{\partial z}\right]^T = \overline{\overline{P}}_e(\lambda, \tilde{z}_i)\overline{\overline{P}}_e(\lambda, -d_{i+1})\cdots\overline{\overline{P}}_e(\lambda, -d_N)[1,0]^T \quad (9)$$

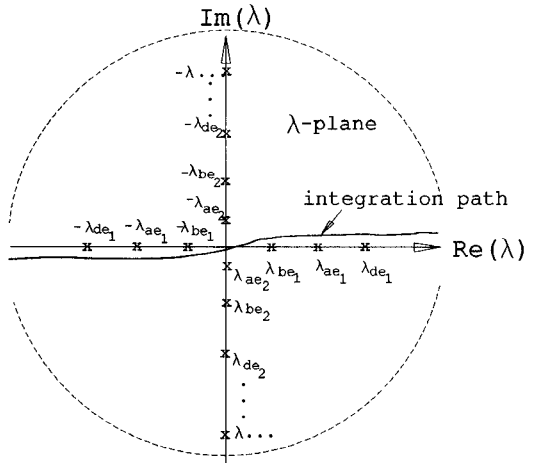


Fig. 3. The integration path in the $\lambda$ plane.

and

$$\left[\psi_{bh}(\lambda,z),\frac{1}{\mu_{r_i}}\frac{\partial\psi_{bh}(\lambda,z)}{\partial z}\right]^T = \overline{\overline{P}}_h(\lambda,\tilde{z}_i)\overline{\overline{P}}_h(\lambda,-d_{i+1})\cdots\overline{\overline{P}}_h(\lambda,-d_N)[0,1]^T \tag{10}$$

where $z_b=\Sigma_{j=-M,J\neq 0}^{i} d_j$, and $\tilde{z}_i = z - z_b$. The superscript $T$ in (7)–(10) is the transpose operator and the column vectors $[1,\ 0]^T$ and $[0,\ 1]^T$ come from the boundary conditions that force the tangential electric fields to vanish on the PECs at $z=0$ and $z=A$.

Similarly, with $\overline{\overline{P}}_e$ and $\overline{\overline{P}}_h$, the following functions $D_{ip}(\lambda)$ whose zeros determine the allowable normalized propagation constants of the PPM's in the $y$ direction for each region with a given $\alpha$, can be constructed. In $D_{ip}(\lambda)$, the subscript $i$ denotes the region ($i$ = 1, 2 or 3), while $p=e$ or $p=h$, denotes the $TM_z$ or $TE_z$ polarization, respectively.

$$\begin{aligned}
D_{1e}(\lambda) &= [0,1]\overline{\overline{P}}_e(\lambda,d_N)\cdots\overline{\overline{P}}_e(\lambda,d_2)\overline{\overline{P}}_e(\lambda,d_1)\\
&\quad\cdot\overline{\overline{P}}_e(\lambda,d_{-1})\overline{\overline{P}}_e(\lambda,d_{-2})\cdots\overline{\overline{P}}_e(\lambda,d_{-M})[1,0]^T\\
D_{2e}(\lambda) &= [0,1]\overline{\overline{P}}_e(\lambda,d_{-1})\overline{\overline{P}}_e(\lambda,d_{-2})\cdots\overline{\overline{P}}_e(\lambda,d_{-M})[1,0]^T\\
D_{3e}(\lambda) &= [0,1]\overline{\overline{P}}_e(\lambda,-d_1)\overline{\overline{P}}_e(\lambda,-d_2)\cdots\\
&\quad\cdot\overline{\overline{P}}_e(\lambda,-d_N)[1,0]^T
\end{aligned} \tag{11}$$

$$\begin{aligned}
D_{1h}(\lambda) &= [1,0]\overline{\overline{P}}_h(\lambda,d_N)\cdots\overline{\overline{P}}_h(\lambda,d_2)\overline{\overline{P}}_h(\lambda,d_1)\\
&\quad\cdot\overline{\overline{P}}_h(\lambda,d_{-1})\overline{\overline{P}}_h(\lambda,d_{-2})\cdots\overline{\overline{P}}_h(\lambda,d_{-M})[0,1]^T\\
D_{2h}(\lambda) &= [1,0]\overline{\overline{P}}_h(\lambda,d_{-1})\overline{\overline{P}}_h(\lambda,d_{-2})\cdots\overline{\overline{P}}_h(\lambda,d_{-M})[0,1]^T\\
D_{3h}(\lambda) &= [1,0]\overline{\overline{P}}_h(\lambda,-d_1)\overline{\overline{P}}_h(\lambda,-d_2)\cdots\\
&\quad\cdot\overline{\overline{P}}_h(\lambda,-d_N)[0,1]^T
\end{aligned} \tag{12}$$

Since $D_{ip}$ is an even function of $\lambda$, the roots $\pm\lambda_{ip_n}, n=1,2,\cdots$ are symmetrically paired with respect to the origin in the $\lambda$ plane, as indicated in Fig. 3. Note that $\lambda_{ip_n}$ lies in the lower half $\lambda$ plane, while $-\lambda_{ip_n}$ in the upper half $\lambda$ plane.

Now let us consider the incident field that is the $m$th $TM_z$ polarized PPM obliquely incident onto the edge of the PEC half plane from region 2; namely,

$$\begin{aligned}
E_z^{inc}(x,y,z) &= \frac{\psi_{de}(-\lambda_m,z)}{\epsilon_r(z)}e^{jk_0\lambda_m y}\\
\mathbf{E_t^{inc}}(x,y,z) &= -\frac{j}{k_0}\frac{(\alpha\hat{\mathbf{x}}-\lambda_m\hat{\mathbf{y}})}{(\alpha^2+\lambda_m^2)}\frac{1}{\epsilon_r(z)}\\
&\quad\cdot\frac{\partial\psi_{de}(-\lambda_m,z)}{\partial z}e^{jk_0\lambda_m y}\\
\mathbf{H_t^{inc}}(x,y,z) &= -\frac{1}{\eta_0}\frac{(\lambda_m\hat{\mathbf{x}}+\alpha\hat{\mathbf{y}})}{(\alpha^2+\lambda_m^2)}\psi_{de}(-\lambda_m,z)e^{jk_0\lambda_m y}
\end{aligned} \tag{13}$$

for $-\infty<y<\infty, 0\leq z<D$; where $\eta_0$ is the intrinsic impedance of free space, the superscript 'inc' denotes the incident fields, while the subscript '$t$' denotes the tangential fields and $\lambda_m$ stands for $\lambda_{2e_m}$ for the sake of brevity. This field can also be referred to as the unperturbed field because it is the field that would exist if the PEC half plane were extended to $y\rightarrow-\infty$.

Usually, in the WH analysis, a small loss in the material is introduced first and then the lossless case is treated as the limiting case of vanishing loss afterwards. Here, the lossless case is considered directly for simplicity. However, this should by no means be a source of confusion. If the dielectric materials are lossless and $\alpha$ is real, then the integration path is along the real $\lambda$ axis, as shown in Fig. 3. The following formulation is based on Jones' method [4], [5].

The total fields are equal to the sum of the incident and scattered fields; namely,

$$\mathbf{E^{tot}}=\mathbf{E^{inc}}+\mathbf{E^s},\ \mathbf{H^{tot}}=\mathbf{H^{inc}}+\mathbf{H^s} \tag{14}$$

where the superscripts 'tot' and 's' denote the total and scattered fields, respectively. Assume the spectral representation of the scattered field for $z<D$ to be

$$\begin{aligned}
\tilde{E}_z^s(\lambda,z) &= E_d(\lambda)\frac{\psi_{de}(\lambda,z)}{\psi_{de}(\lambda,D)}\\
\tilde{H}_z^s(\lambda,z) &= H_d(\lambda)\frac{\psi_{dh}(\lambda,z)}{\psi_{dh}(\lambda,D)}\\
\tilde{\mathbf{E}}_\mathbf{t}^\mathbf{s}(\lambda,z) &= -\frac{j}{k_0}\frac{(\alpha\hat{\mathbf{x}}+\lambda\hat{\mathbf{y}})}{(\alpha^2+\lambda^2)}E_d(\lambda)\frac{\frac{\partial}{\partial z}\psi_{de}(\lambda,z)}{\psi_{de}(\lambda,D)}\\
&\quad-\eta_0\frac{(\lambda\hat{\mathbf{x}}-\alpha\hat{\mathbf{y}})}{(\alpha^2+\lambda^2)}\mu_r(z)H_d(\lambda)\frac{\psi_{dh}(\lambda,z)}{\psi_{dh}(\lambda,D)}\\
\tilde{\mathbf{H}}_\mathbf{t}^\mathbf{s}(\lambda,z) &= \frac{1}{\eta_0}\frac{(\lambda\hat{\mathbf{x}}-\alpha\hat{\mathbf{y}})}{(\alpha^2+\lambda^2)}\epsilon_r(z)E_d(\lambda)\frac{\psi_{de}(\lambda,z)}{\psi_{de}(\lambda,D)}\\
&\quad-\frac{j}{k_0}\frac{(\alpha\hat{\mathbf{x}}+\lambda\hat{\mathbf{y}})}{(\alpha^2+\lambda^2)}H_d(\lambda)\frac{\frac{\partial}{\partial z}\psi_{dh}(\lambda,z)}{\psi_{dh}(\lambda,D)}
\end{aligned} \tag{15}$$

and for $z>D$,

$$\tilde{E}_z^s(\lambda,z)=E_b(\lambda)\frac{\psi_{be}(\lambda,z)}{\psi_{be}(\lambda,D)}$$

$$\tilde{H}_z^s(\lambda,z) = H_b(\lambda)\frac{\psi_{bh}(\lambda,z)}{\psi_{bh}(\lambda,D)}$$

$$\tilde{\mathbf{E}}_t^s(\lambda,z) = -\frac{j}{k_0}\frac{(\alpha\hat{\mathbf{x}}+\lambda\hat{\mathbf{y}})}{(\alpha^2+\lambda^2)}E_b(\lambda)\frac{\frac{\partial}{\partial z}\psi_{be}(\lambda,z)}{\psi_{be}(\lambda,D)} - \eta_0\frac{(\lambda\hat{\mathbf{x}}-\alpha\hat{\mathbf{y}})}{(\alpha^2+\lambda^2)}\mu_r(z)H_b(\lambda)\frac{\psi_{bh}(\lambda,z)}{\psi_{bh}(\lambda,D)}$$

$$\tilde{\mathbf{H}}_t^s(\lambda,z) = \frac{1}{\eta_0}\frac{(\lambda\hat{\mathbf{x}}-\alpha\hat{\mathbf{y}})}{(\alpha^2+\lambda^2)}\epsilon_r(z)E_b(\lambda)\frac{\psi_{be}(\lambda,z)}{\psi_{be}(\lambda,D)} - \frac{j}{k_0}\frac{(\alpha\hat{\mathbf{x}}+\lambda\hat{\mathbf{y}})}{(\alpha^2+\lambda^2)}H_b(\lambda)\frac{\frac{\partial}{\partial z}\psi_{bh}(\lambda,z)}{\psi_{bh}(\lambda,D)} \quad (16)$$

where $\epsilon_r(z)$ and $\mu_r(z)$ are piecewise constant functions which assume the values $\epsilon_{r_i}$ and $\mu_{r_i}$, respectively, in the $i$th layer. $E_d(\lambda), H_d(\lambda), E_b(\lambda)$ and $H_b(\lambda)$ are the unknown functions to be solved. The scattered fields in (15) and (16) already satisfy the boundary condition for the PECs at $z=0$ and $z=A$ and as well as the continuity condition at the interface between any two dielectric layers for regions $z<D$ and $z>D$. The remaining condition that needs to be enforced is at $z=D$ where the PEC half plane resides; namely,

$$\mathbf{E}_t^{\mathbf{tot}}(y,z=D) = 0; \qquad 0<y<\infty \quad (17)$$

$$\mathbf{E}_t^{\mathbf{tot}}(y,z=D_-) = \mathbf{E}_t^{\mathbf{tot}}(y,z=D_+); \qquad -\infty<y<0 \quad (18)$$

$$\mathbf{H}_t^{\mathbf{tot}}(y,z=D_-) = \mathbf{H}_t^{\mathbf{tot}}(y,z=D_+); \qquad -\infty<y<0 \quad (19)$$

along with the edge condition near $y=0, z=D$ and the radiation condition for $y\to\infty$ and $-\infty$. With all the functions defined above, the scattering problem of a PPM by a PEC half plane embedded in a multilayered dielectric region is reduced to a formulation that is similar to the corresponding single-layered one.

Notice that in the spectral domain, the $\mathrm{TM}_z$ and $\mathrm{TE}_z$ potentials always give rise to tangential fields that are in one of the following two mutually orthogonal directions for fixed $\alpha$ and $\lambda$; namely,

$$\hat{\mathbf{u}} = \frac{(\lambda\hat{\mathbf{x}}-\alpha\hat{\mathbf{y}})}{\sqrt{\alpha^2+\lambda^2}}, \hat{\mathbf{v}} = \frac{(\alpha\hat{\mathbf{x}}+\lambda\hat{\mathbf{y}})}{\sqrt{\alpha^2+\lambda^2}}. \quad (20)$$

This property, which is also important in deriving the Green's functions in the SDA [10], [13], makes the decoupling of the boundary conditions at $z=D$ possible.

Boundary conditions (17) and (18) together imply that

$$\tilde{\mathbf{E}}_t^s(\lambda,z=D_-) = \tilde{\mathbf{E}}_t^s(\lambda,z=D_+), \quad (21)$$

since $\mathbf{E}_t^{\mathbf{inc}}(y,z=D_-) = \mathbf{E}_t^{\mathbf{inc}}(y,z=D_+) = 0$ for $-\infty<y<\infty$. From (15) and (16), one obtains two relations

$$\frac{\epsilon_{r_{-1}}E_d(\lambda)D_{3e}(\lambda)}{\psi_{de}(\lambda,D)} = \frac{\epsilon_{r_1}E_b(\lambda)D_{2e}(\lambda)}{\psi_{be}(\lambda,D)} \quad (22)$$

and

$$\mu_{r_{-1}}H_d(\lambda) = \mu_{r_1}H_b(\lambda). \quad (23)$$

The boundary condition (19) can be written as

$$\mathbf{H}_t^{\mathbf{tot}}(y,z=D_+) - \mathbf{H}_t^{\mathbf{tot}}(y,z=D_-) = -\hat{z}\times\mathbf{J}_s^{\mathbf{tot}}(y), \qquad -\infty<y<\infty \quad (24)$$

where $\mathbf{J}_s^{\mathbf{tot}}(y)$ is the total induced surface current on the PEC half plane, which can be written as the sum of two portions:

$$\mathbf{J}_s^{\mathbf{tot}}(y) = \begin{cases}\mathbf{J}_s^{\mathbf{inc}}(y)+\mathbf{J}_s^{\mathbf{s}}(y), & y>0\\ 0, & y<0\end{cases} \quad (25)$$

The first portion $\mathbf{J}_s^{\mathbf{inc}}(y)$ is the surface current induced by the incident field and defined as

$$\mathbf{J}_s^{\mathbf{inc}}(y) = \begin{cases}-\hat{z}\times\mathbf{H}_t^{\mathbf{inc}}(y,z=D_-), & y>0\\ 0, & y<0\end{cases} \quad (26)$$

The other portion $\mathbf{J}_s^{\mathbf{s}}(y)$ is the unknown surface current induced by the scattered field. Substituting (25) and (26) into (24) and taking the Fourier transform yields

$$\tilde{\mathbf{H}}_t^s(\lambda,z=D_+) - \tilde{\mathbf{H}}_t^s(\lambda,z=D_-) = \tilde{\mathbf{H}}_{t_-}^{\mathbf{inc}}(\lambda,z=D_-) - \hat{z}\times\tilde{\mathbf{J}}_{s_+}^{\mathbf{s}}(\lambda) \quad (27)$$

where the subscripts '+' and ' −' denote the one-sided Fourier transformed functions and

$$\tilde{\mathbf{H}}_{t_-}^{\mathbf{inc}}(\lambda,z=D_-) = \frac{j}{2\pi}\frac{1}{\eta_0}\frac{(\lambda_m\hat{\mathbf{x}}+\alpha\hat{\mathbf{y}})}{(\alpha^2+\lambda_m^2)}\frac{\psi_{de}(-\lambda_m,D)}{(\lambda+\lambda_m)} \quad (28)$$

from (13) and (3). Equation (27) actually involves two scalar equations since it is in a vector form. Applying (27) in the $\hat{\mathbf{u}}$ direction and using (22) and (28) gives

$$\frac{\epsilon_{r_1}E_b(\lambda)D_{2e}(\lambda)}{k_0\psi_{be}(\lambda,D)Q_e(\lambda)} = \frac{-j}{2\pi}\left(\frac{1}{\lambda+\lambda_m}-\frac{\lambda_m}{\alpha^2+\lambda_m^2}\right)\psi_{de}(-\lambda_m,D) + \eta_0(\alpha\hat{\mathbf{x}}+\lambda\hat{\mathbf{y}})\cdot\tilde{\mathbf{J}}_{s_+}^{\mathbf{s}}(\lambda) \quad (29)$$

where

$$Q_e(\lambda) = \frac{D_{2e}(\lambda)D_{3e}(\lambda)}{k_0D_{1e}(\lambda)} = Q_{e_+}(\lambda)Q_{e_-}(\lambda). \quad (30)$$

Similarly, applying (27) in the $\hat{\mathbf{v}}$ direction and using (23) and (28) gives

$$\frac{-j\mu_{r_1}H_b(\lambda)}{Q_h(\lambda)} = \frac{j}{2\pi}\frac{1}{\eta_0}\frac{\alpha}{(\alpha^2+\lambda_m^2)}\psi_{de}(-\lambda_m,D) + (-\lambda\hat{\mathbf{x}}+\alpha\hat{\mathbf{y}})\cdot\tilde{\mathbf{J}}_{s_+}^{\mathbf{s}}(\lambda) \quad (31)$$

where

$$Q_h(\lambda) = \frac{k_0D_{2h}(\lambda)D_{3h}(\lambda)}{D_{1h}(\lambda)} = Q_{h_+}(\lambda)Q_{h_-}(\lambda). \quad (32)$$

$Q_e(\lambda)$ and $Q_h(\lambda)$, which are closely related to the Green's function kernels for the multilayered dielectric slab, are functions to be factorized. The representation of $Q_{e,h}$ as a product of two functions $Q_{e_+,h_+}$ and $Q_{e_-,h_-}$, which are regular and free of zeros in the upper and lower half $\lambda$ planes, respectively, is referred to as the factorization of $Q_{e,h}$. Since all the $D_{ip}(\lambda)\,(i=1,2,3;\ p=e,h)$ are regular and even functions of $\lambda$ with simple zeros, the factorization is simple

and the result is given in the appendix. Equations (29) and (31) are the two WH equations that need to be solved. The boundary condition (17) implies that $\tilde{\mathbf{E}}_{\mathbf{t}}^{\mathbf{s}}$ is regular in the lower half $\lambda$ plane, or equivalently, $E_b(\lambda)D_{2e}(\lambda)/\psi_{be}(\lambda, D)$ and $H_b(\lambda)$ are regular in the lower half plane. From the edge condition [4], we have $E_b(\lambda) \sim \lambda^{-p}, H_b(\lambda) \sim \lambda^{-p}, \tilde{\mathbf{J}}_{\mathbf{s}_+}^{\mathbf{s}} \cdot \hat{\mathbf{u}} \sim \lambda^{-p}, \tilde{\mathbf{J}}_{\mathbf{s}_+}^{\mathbf{s}} \cdot \hat{\mathbf{v}} \sim \lambda^{-1-p}$ as $|\lambda| \to \infty$ where $0 < p < 1$. Also, from (11), (12), (30), and (32), it follows that $Q_e(\lambda) \sim \lambda, Q_h(\lambda) \sim \lambda^{-1}, D_{2e}(\lambda)/\psi_{be}(\lambda, D) \sim \lambda$ as $|\lambda| \to \infty$. Thus, both (29) and (31) can be written into a standard form of the WH equations where one side of the equation is regular in the lower half $\lambda$ plane while the other side is regular in the upper half $\lambda$ plane. Note that there must be an overlapping region between these two half planes, which is the real axis of the $\lambda$ plane if $\alpha$ is real and all the dielectrics are lossless. By rearranging (29) and (31), examining the behavior of various terms and invoking Liouville's theorem [4], one obtains

$$\begin{aligned}
&\frac{\epsilon_{r_1} E_b D_{2e}(\lambda)}{k_0 \psi_{be}(\lambda, D) Q_{e_-}(\lambda)} + \frac{j}{2\pi} \frac{1}{(\lambda + \lambda_m)} \\
&\qquad \cdot \psi_{de}(-\lambda_m, D) Q_{e_+}(-\lambda_m) \\
&\quad = -\frac{j}{2\pi} \frac{\psi_{de}(-\lambda_m, D)}{(\lambda + \lambda_m)} \left(Q_{e_+}(\lambda) - Q_{e_+}(-\lambda_m)\right) \\
&\qquad + \frac{j}{2\pi} \frac{\lambda_m}{(\alpha^2 + \lambda_m^2)} \psi_{de}(-\lambda_m, D) Q_{e_+}(\lambda) \\
&\qquad + \eta_0 (\alpha \hat{\mathbf{x}} + \lambda \hat{\mathbf{y}}) \cdot \tilde{\mathbf{J}}_{\mathbf{s}_+}^{\mathbf{s}} Q_{e_+}(\lambda) \\
&\quad = \frac{j}{2\pi} \psi_{de}(-\lambda_m, D) Q_{e_+}(-\lambda_m) C_1 \qquad (33)
\end{aligned}$$

and

$$\begin{aligned}
\frac{-j\mu_{r_1} H_b}{Q_{h_-}(\lambda)} &= \frac{j}{2\pi} \frac{1}{\eta_0} \frac{\alpha}{(\alpha^2 + \lambda_m^2)} \psi_{de}(-\lambda_m, D) Q_{h_+}(\lambda) \\
&\quad + (-\lambda \hat{\mathbf{x}} + \alpha \hat{\mathbf{y}}) \cdot \tilde{\mathbf{J}}_{\mathbf{s}_+}^{\mathbf{s}} Q_{h_+}(\lambda) \\
&= -\frac{1}{2\pi\eta_0} \psi_{de}(-\lambda_m, D) Q_{e_+}(-\lambda_m) C_2 \qquad (34)
\end{aligned}$$

where $C_1$ and $C_2$ are constants to be determined. Equations (33) and (34) yield

$$\begin{aligned}
\frac{\epsilon_{r_1} E_b(\lambda) D_{2e}(\lambda)}{k_0 \psi_{be}(\lambda, D)} &= \frac{j}{2\pi} \psi_{de}(-\lambda_m, D) Q_{e_+}(-\lambda_m) \\
&\quad \cdot \left(C_1 - \frac{1}{\lambda + \lambda_m}\right) Q_{e_-}(\lambda) \qquad (35)
\end{aligned}$$

and

$$\begin{aligned}
\mu_{r_1} H_b(\lambda) &= -\frac{j}{2\pi\eta_0} \psi_{de}(-\lambda_m, D) Q_{e_+}(-\lambda_m) \\
&\quad \cdot C_2 Q_{h_-}(\lambda) \qquad (36)
\end{aligned}$$

The remaining task is to find the two unknown constants $C_1$ and $C_2$. Substituting (35) and (36) into (16), and using the condition that $\tilde{\mathbf{E}}_{\mathbf{t}}^{\mathbf{s}}(\lambda, D)$ is regular in the lower half $\lambda$ plane and thus cannot have a pole at $\lambda = -j\alpha$, yields

$$C_1 Q_{e_+}(j\alpha) + C_2 Q_{h_+}(j\alpha) = \frac{Q_{e_+}(j\alpha)}{(-j\alpha + \lambda_m)}. \qquad (37)$$

Also, expressing $\tilde{\mathbf{J}}_{\mathbf{s}_+}^{\mathbf{s}}(\lambda)$ as a sum of its components in the $\hat{\mathbf{u}}$ and $\hat{\mathbf{v}}$ directions, which can be obtained from (33) and (34), and then requiring that $\tilde{\mathbf{J}}_{\mathbf{s}_+}^{\mathbf{s}}(\lambda)$ be regular in the upper half plane, which implies that $\tilde{\mathbf{J}}_{\mathbf{s}_+}^{\mathbf{s}}(\lambda)$ cannot have a pole at $\lambda = j\alpha$, yields

$$\frac{C_1}{Q_{e_+}(j\alpha)} + \frac{C_2}{Q_{h_+}(j\alpha)} = \frac{1}{(j\alpha + \lambda_m) Q_{e_+}(j\alpha)}. \qquad (38)$$

Thus, $C_1$ and $C_2$ can be solved as

$$C_1 = \frac{\lambda_m}{(\lambda_m^2 + \alpha^2)} + \frac{j\alpha}{(\lambda_m^2 + \alpha^2)} \Omega_1 \qquad (39)$$

and

$$C_2 = -\frac{j\alpha}{(\lambda_m^2 + \alpha^2)} \Omega_2 \qquad (40)$$

where

$$\Omega_1 = \frac{Q_{e_+}^2(j\alpha) + Q_{h_+}^2(j\alpha)}{Q_{e_+}^2(j\alpha) - Q_{h_+}^2(j\alpha)} \qquad (41)$$

and

$$\Omega_2 = \frac{2 Q_{e_+}(j\alpha) Q_{h_+}(j\alpha)}{Q_{e_+}^2(j\alpha) - Q_{h_+}^2(j\alpha)}. \qquad (42)$$

Substituting the result of $C_1$ and $C_2$ back to (35) and (36), the expressions for the functions $E_b(\lambda)$ and $H_b(\lambda)$ are obtained. $E_d(\lambda)$ and $H_d(\lambda)$ can be then be deduced from (22) and (23), respectively. Consequently, all the terms for the scattered fields in the spectral domain as defined in (15) and (16) are known. The last step is to take the inverse Fourier transforms to obtain the scattered fields in the spatial domain. This inversion integral can be evaluated using the Cauchy Residue Theorem after closing the original integration path (along the real $\lambda$ axis) by a half circle of an infinitely large radius in the lower half $\lambda$ plane when $y > 0$, and likewise in the upper half $\lambda$ plane when $y < 0$.

### *B. Generalized Scattering Matrix for the Half-Plane*

To completely characterize the scattering properties of the half-plane configuration depicted in Fig. 2, it is necessary to consider six cases, namely, the incidence of a PPM from each of the three regions where the PPM is either $\mathrm{TM}_z$ or $\mathrm{TE}_z$ polarized. The analysis of one case was presented in the previous subsection; however, the analytical details of the other five cases will not be discussed here because they are similar to the one considered above. Thus, after solving six canonical scattering problems, the generalized scattering matrix that characterizes the PEC half plane edge discontinuity can be written down. Let the $z$-components of the total electric and magnetic fields in different regions be expressed as follows:

$$\begin{aligned}
E_z(y, z) &= \sum_n [A_{1n}^+ e^{jk_0 \lambda_{1e_n} y} + A_{1n}^- e^{-jk_0 \lambda_{1e_n} y}] e_{1n} \\
H_z(y, z) &= \sum_n [B_{1n}^+ e^{jk_0 \lambda_{1h_n} y} + B_{1n}^- e^{-jk_0 \lambda_{1h_n} y}] h_{1n}
\end{aligned} \qquad (43)$$

if $y<0$ and

$$E_z(y,z)=\sum_n[A_{in}^+e^{-jk_0\lambda_{ie_n}y}+A_{in}^-e^{jk_0\lambda_{ie_n}y}]e_{in},$$
$$H_z(y,z)=\sum_n[B_{in}^+e^{-jk_0\lambda_{ih_n}y}+B_{in}^-e^{jk_0\lambda_{ih_n}y}]h_{in} \tag{44}$$

where $i=2$ if $y>0, z<D$ and $i=3$ if $y>0, z>D$. The modal functions $e_{in}$ and $h_{in}$ for the $n$th TM$_z$ and TE$_z$ PPM's in region $i$ are given by

$$e_{1n}=\frac{\psi_{de}(\lambda_{1e_n},z)}{\epsilon_r(z)},\quad e_{2n}=\frac{\psi_{de}(\lambda_{2e_n},z)}{\epsilon_r(z)},$$
$$e_{3n}=\frac{\psi_{be}(\lambda_{3e_n},z)}{\epsilon_r(z)} \tag{45}$$

and

$$h_{1n}=\frac{\psi_{dh}(\lambda_{1h_n},z)}{\mu_r(z)},\quad h_{2n}=\frac{\psi_{dh}(\lambda_{2h_n},z)}{\mu_r(z)},$$
$$h_{3n}=\frac{\psi_{bh}(\lambda_{3h_n},z)}{\mu_r(z)}. \tag{46}$$

The edge can be viewed as a three-port circuit where the scattering matrix $[S]$ is defined below.

$$[([A_1^+],[B_1^+]),([A_2^+],[B_2^+]),([A_3^+],[B_3^+])]^T$$
$$=[S][([A_1^-],[B_1^-]),([A_2^-],[B_2^-]),([A_3^-],[B_3^-])]^T \tag{47}$$

where

$$[A_i^\pm]=[A_{i1}^\pm,A_{i2}^\pm\cdots A_{in}^\pm\cdots],$$
$$[B_i^\pm]=[B_{i1}^\pm,B_{i2}^\pm\cdots B_{in}^\pm\cdots],\qquad i=1,2,3. \tag{48}$$

The matrix $[S]$ consists of nine blocks of submatrices $[S_{ij}]$; namely,

$$[S]=\begin{bmatrix}[S_{11}] & [S_{12}] & [S_{13}]\\ [S_{21}] & [S_{22}] & [S_{23}]\\ [S_{31}] & [S_{32}] & [S_{33}]\end{bmatrix}, \tag{49}$$

where each block $[S_{ij}]$ contains four submatrices,

$$[S_{ij}]=\begin{bmatrix}[S_{ie,je}] & [S_{ie,jh}]\\ [S_{ih,je}] & [S_{ih,jh}]\end{bmatrix}. \tag{50}$$

After lengthy algebraic manipulations, it turns out that all the elements of the 36 submatrices can be expressed in a single compact form instead of listing them case by case. Namely, the $m$th row, $n$th column element of the submatrix $[S_{ip,jq}]$, denoted by $S_{ip,jq}(m,n)$, is given by

$$S_{ip,jq}(m,n)=\Psi_{ip}(m)\mathcal{F}(m,n;ip,jq)\Phi_{jq}(n) \tag{51}$$

$i,j=1,2$ or 3; $p,q=e$ or $h$; $m,n=1,2,3\cdots$, where

$$\Psi_{1e}(m)=-D_{2e}(-\lambda_{1e_m})\Big/\frac{d}{d\lambda}D_{1e}(\lambda=-\lambda_{1e_m})$$
$$\Psi_{1h}(m)=-k_0D_{2h}(-\lambda_{1h_m})\Big/\frac{d}{d\lambda}D_{1h}(\lambda=-\lambda_{1h_m})$$
$$\Psi_{2e}(m)=k_0\Big/\frac{d}{d\lambda}D_{2e}(\lambda=\lambda_{2e_m})$$
$$\Psi_{2h}(m)=1\Big/\frac{d}{d\lambda}D_{2h}(\lambda=\lambda_{2h_m})$$
$$\Psi_{3e}(m)=k_0\Big/\frac{d}{d\lambda}D_{3e}(\lambda=\lambda_{3e_m})$$
$$\Psi_{3h}(m)=1\Big/\frac{d}{d\lambda}D_{3h}(\lambda=\lambda_{3h_m}). \tag{52}$$

The function $\mathcal{F}(m,n;ip,jq)$ consists of two parts,

$$\mathcal{F}(m,n;ip,jq)=\mathcal{F}_1(m,n;ip,jq)\mathcal{F}_2(m,n;ip,jq), \tag{53}$$

where the first part $\mathcal{F}_1(m,n;ip,jq)$ is the product of two $Q_+$ functions,

$$\mathcal{F}_1(m,n;ip,jq)=\begin{Bmatrix}Q_{p_+}(-\lambda_{ip_m}) & \text{if} & i=2,3\\ 1/Q_{p_+}(-\lambda_{ip_m}) & \text{if} & i=1\end{Bmatrix}\cdot\begin{Bmatrix}Q_{q_+}(-\lambda_{jq_n}) & \text{if} & j=2,3\\ 1/Q_{q_+}(-\lambda_{jq_n}) & \text{if} & j=1\end{Bmatrix} \tag{54}$$

and the second part $\mathcal{F}_2(m,n;ip,jq)$ is given by

$$\mathcal{F}_2(m,n;ip,jq)=\begin{cases}[\lambda_R\lambda_I-\alpha^2+j\alpha(\lambda_R+\lambda_I)\Omega_1]/(\lambda_R+\lambda_I)/(\alpha^2+\lambda_I^2)\\ \quad\text{if}\quad (p,q)=(e,e)\\ j\alpha\Omega_2/\eta_0/(\alpha^2+\lambda_I^2)\quad\text{if}\quad (p,q)=(h,e)\\ -j\alpha\Omega_2\eta_0/(\alpha^2+\lambda_I^2)\quad\text{if}\quad (p,q)=(e,h)\\ [\lambda_R\lambda_I-\alpha^2-j\alpha(\lambda_R+\lambda_I)\Omega_1]/(\lambda_R+\lambda_I)/(\alpha^2+\lambda_I^2)\\ \quad\text{if}\quad (p,q)=(h,h)\end{cases} \tag{55}$$

where

$$\lambda_R=\begin{cases}\lambda_{ip_m} & \text{if } i=2,3;\\ -\lambda_{ip_m} & \text{if } i=1\end{cases}$$
$$\lambda_I=\begin{cases}\lambda_{jq_n} & \text{if } j=2,3\\ -\lambda_{jq_n} & \text{if } j=1\end{cases} \tag{56}$$

The functions $\Phi_{jq}(n)$ are given below.

$$\Phi_{1e}(n)=\frac{1}{k_0}\frac{1}{\epsilon_{r_{-1}}}\frac{\partial}{\partial z}\psi_{de}(\lambda_{1e_n},z=D)$$
$$\Phi_{1h}(n)=\psi_{dh}(\lambda_{1h_n},z=D)$$
$$\Phi_{2e}(n)=\psi_{de}(-\lambda_{2e_n},z=D)$$
$$\Phi_{2h}(n)=\frac{1}{k_0}\frac{1}{\mu_{r_{-1}}}\frac{\partial}{\partial z}\psi_{dh}(-\lambda_{2h_n},z=D)$$
$$\Phi_{3e}(n)=-\psi_{be}(-\lambda_{3e_n},z=D)$$
$$\Phi_{3h}(n)=-\frac{1}{k_0}\frac{1}{\mu_{r_1}}\frac{\partial}{\partial z}\psi_{bh}(-\lambda_{3h_n},z=D). \tag{57}$$

## III. Transverse Resonance Relations

After solving the canonical half-plane scattering problem, the second part of the WH/GSMT scheme is to build the transverse resonance relation via the GSMT [3], [4], [14], [15]. Take the single microstrip line as an example. The cross-section is depicted in Fig. 4(a), where $[a_i]$ and $[b_i]$ are vectors consisting of the amplitudes of both the TM$_z$ and TE$_z$ polarized PPM's, including all the propagating and leading evanescent PPM's. The arrows indicate the lateral direction of wave propagation while the vertical dotted lines

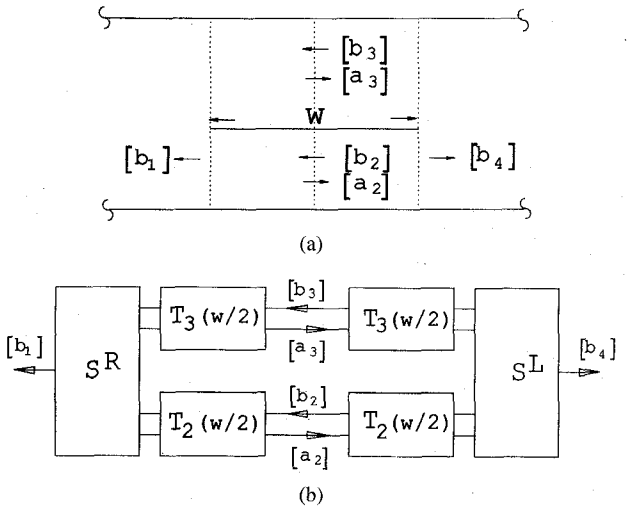


Fig. 4. (a) Cross-section of a single microstrip line and (b) the equivalent network model.

indicate the reference planes for defining $[a_i], [b_i]$ and the scattering matrices. Assume that all the fields have the $e^{-jk_0\alpha x}$ dependence in the longitudinal $x$-direction, where $\alpha$ is the normalized modal propagation constant of the microstrip line to be found. The microstrip line can then be viewed as two discontinuities connected by two uniform transmission lines of length $w$, one above and the other below the strip, as depicted in Fig. 4(b). The scattering matrix $[S^R]$ in Fig. 4(b) is the $[S]$ matrix obtained in Section II while the matrix $[S^L]$ has a sign difference in the elements corresponding to the cross-polarized fields; namely,

$$S^L_{ip,jq}(m,n) = S^R_{ip,jq}(m,n) \quad \text{if } (p,q) = (e,e) \text{ or } (h,h) \tag{58}$$

$$S^L_{ip,jq}(m,n) = -S^R_{ip,jq}(m,n) \quad \text{if } (p,q) = (e,h) \text{ or } (h,e) \tag{59}$$

The matrices $[T_3(w/2)]$ and $[T_2(w/2)]$ in Fig. 4(b) are diagonal matrices that represent the phase change for a distance $w/2$ of the PPM's in the parallel plate waveguide region above and below the conductor strip, respectively. After rearranging the equations and eliminating some unknowns, one obtains the transverse resonance relation as follows [3], [4]:

$$\begin{bmatrix} [I] - [S^C_{22}], & -[S^C_{23}] \\ -[S^C_{32}], & [I] - [S^C_{33}] \end{bmatrix} \begin{bmatrix} [a_2] \\ [a_3] \end{bmatrix} = [0] \tag{60}$$

where $[I]$ is the identity matrix and

$$[S^C_{ij}] = \sum_{k=2}^{3} [T_i(w/2)][S^R_{ik}][T_k(w)][S^L_{kj}][T_j(w/2)], \tag{61}$$

All the matrices $[S^R], [S^L], [T_2]$ and $[T_3]$ above are functions of $\alpha$. The condition that the determinant of (60) vanishes in order to have a nontrivial solution yields the desired values of $\alpha$. Therefore, similar to the SDA, the WH/GSMT yields a matrix where the zeros of its determinant have to be determined numerically. In the WH/GSMT, the corresponding eigenvector yields the amplitudes of the PPM's while in the SDA, it gives the amplitudes of the current basis functions. Actually, it can be said that the WH/GSMT employs inhomogeneous plane waves (PPM's) as the field basis functions. The transverse resonance relation for other planar transmission line configurations can be obtained in a similar way and it will not be shown here.

## IV. Numerical Results

Numerical results based on the WH/GSMT scheme are presented for various planar microwave/millimeter wave transmission lines. There are two kinds of parameters one needs to choose when applying the WH/GSMT. The first one is the number of terms, denoted by $N_{ip}$, which is used for calculating the infinite product $\mathcal{P}_{ip}(i = 1, 2, 3;\ p = e, h)$ in (72) and (74). Usually, these numbers are not very critical as long as they are large enough. The situation is similar to truncating the Sommerfeld integral over the semi-infinite range in the SDA. Although the relative convergence phenomenon is not particularly observed, the rule $N_{1p}/A \sim N_{2p}/D \sim N_{3p}/B$, which is required if the mode matching method is applied, is still recommended. For most of the cases, $N_{ip}$ is smaller than 100. The second set of parameters are the number of PPM's retained in each region, which is analogous to the number of basis functions used in the SDA. These numbers can be estimated from the asymptotic behavior of $\lambda_{ip_n}$ given in (68).

The accuracy of the WH/GSMT method is assessed by comparing the results based on this method with those available in the literature. $Re[\alpha]$ and $Im[\alpha]$ denote the normalized phase constant and normalized attenuation constant, respectively. For the sake of convenience, the sign of $Im[\alpha]$ is neglected in the results shown.

### A. Single Microstrip Line (SMS)

A wide SMS that was previously studied by Ermert [16], [17] and Oliner *et al.* [6], [7] is considered in the first example. $Re[\alpha]$ and $Im[\alpha]$ are plotted as functions of frequency in Fig. 5 where the curves for $N = 0$, 1 and 2 correspond to the dominant, first and second higher-order modes, respectively. The dashed line in the $Re[\alpha]$ of Fig. 5 is the normalized phase constant of the lowest order PPM between the top and bottom PEC planes, which will become the $TM_0$ surface wave when the top cover is removed. The two dotted lines correspond to values of $\sqrt{\epsilon_{r1}}$ and $\sqrt{\epsilon_{r2}}$, respectively. The dashed line and the $\sqrt{\epsilon_{r2}} = 1$ dotted line are the thresholds of surface wave leakage and space wave radiation, respectively, when the top cover is removed. As shown in Fig. 5 the dominant mode is bounded for all frequencies since most of the fields are concentrated under the strip and thus have a higher effective dielectric constant. As the frequency increases, $Re[\alpha]$ of this mode will approach the limit $\sqrt{\epsilon_{r1}}$. The first and second higher-order modes will have power leakage in the lateral directions when their phase velocities are faster than that of the PPM; the cut-off frequency for these higher order modes is around 14.5 and 29.0 GHz, respectively.

Since the microstrip line is relatively wide, only 1 and 2 evanescent PPM's are used for the region above and below the strip, respectively, and $N_{1p} = 18, N_{2p} = 4, N_{3p} = 14; p = e, h$. The curves for $Re[\alpha]$ shown in Fig. 5 agree with [6] where a simplified model is used, while $Im[\alpha]$ tends to be larger

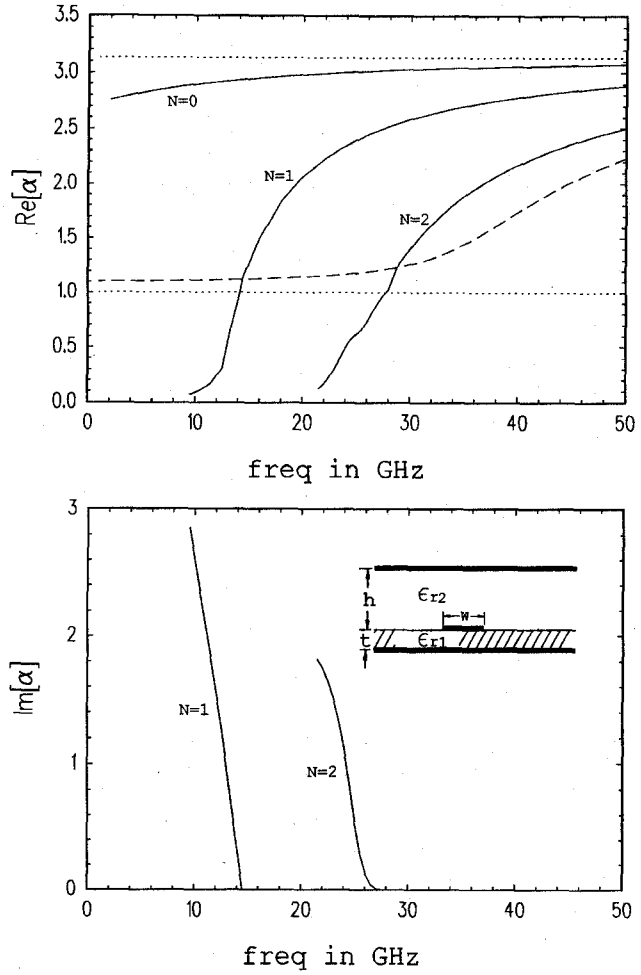


Fig. 5. The normalized phase constant $Re[\alpha]$ and attenuation constant $Im[\alpha]$ of a SMS versus frequency. $\epsilon_{r1} = 9.8, \epsilon_{r2} = 1.0, w = 3.0$ mm, $t = 0.635$ mm, $h = 2.54$ mm.

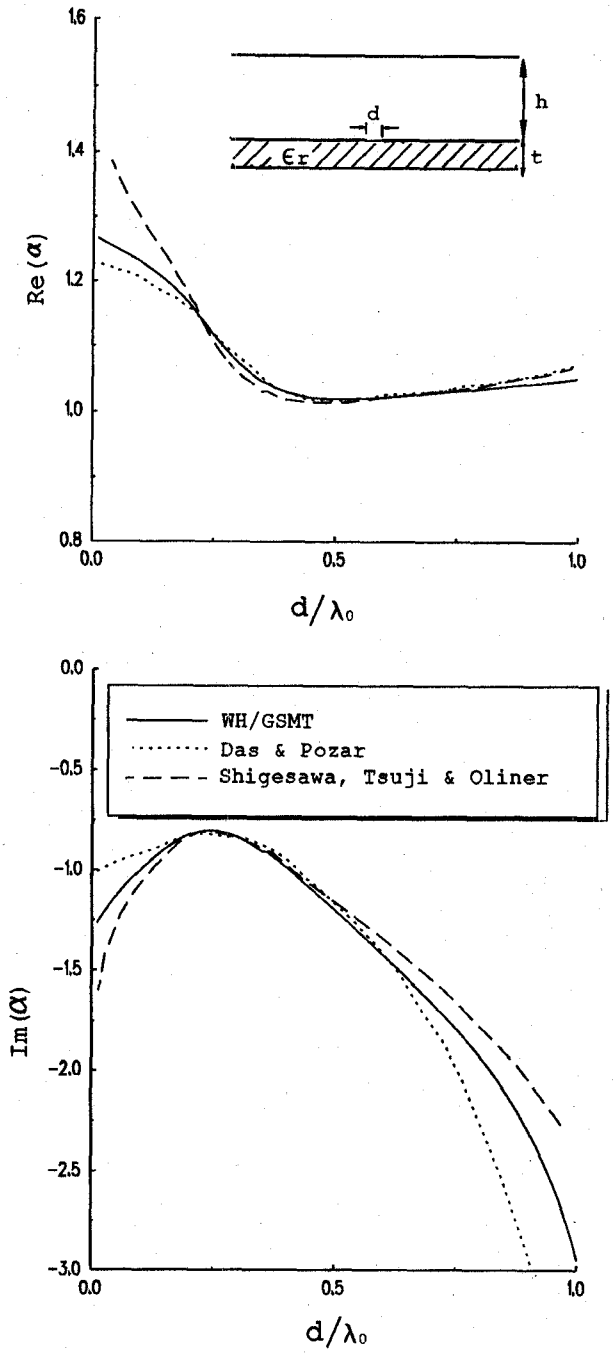


Fig. 6. The normalized phase constant $Re[\alpha]$ and attenuation constant $Im[\alpha]$ versus the normalized slot width $d/\lambda_0$. $\epsilon_r = 2.25$, $t/\lambda_0 = 0.267, h/\lambda_0 = 3.33$.

than that given in [6]. Note that it is usually more difficult to achieve the same accuracy for Im $[\alpha]$ than $Re[\alpha]$.

### *B. Single Slotline (SSL)*

$Re[\alpha]$ and $Im[\alpha]$ of a single conductor-backed slotline as functions of the normalized slot width $d/\lambda_0$ are given in Fig. 6 where the solid line is obtained by the WH/GSMT while the dotted and the dashed lines are calculated with the spectral domain approach [11] and the spatial domain mode matching method [20], respectively. The results based on these three different methods generally agree well for both the real and imaginary parts of $\alpha$. The deviation when $d/\lambda_0$ is small or large is probably due to the numerical disadvantage inherent in the method used; namely, the spectral domain approach will require a large number of basis functions when the slot width $d$ is large while for the spatial domain mode-matching method and the WH/GSMT, many evanescent PPM's have to be included when $d$ is very small. In this case, $N_{1p} = 50, N_{2p} = 20, N_{3p} = 30; p = e, h$ and five evanescent PPM's are used in the slot region.

### *C. Coupled Microstrip Lines (CMS)*

In Fig. 7, the even and odd mode dispersion characteristics for three different types of CMS are given where the solid, dashed and dotted lines are for conventional CMS, CMS with dielectric overlay, and inverted CMS, respectively. Although the top PEC cover is put infinitely far in [18], the result in Fig. 7 shows good agreement with [18] with $H_3 = 4H_1$. For the overlayed CMS, the normalized phase constants of the even and odd mode are both quite close to $\sqrt{\epsilon_{r1}} (= \sqrt{\epsilon_{r2}})$ for all the frequencies because most of the fields are confined in those two dielectric layers. The dispersion curve for the inverted CMS has the largest variation among the three types of CMS for the range of frequencies considered. In this case, $N_{1p} = 40, N_{2p} = 8, N_{3p} = 35; p = e, h$ and 7, 3, and 5

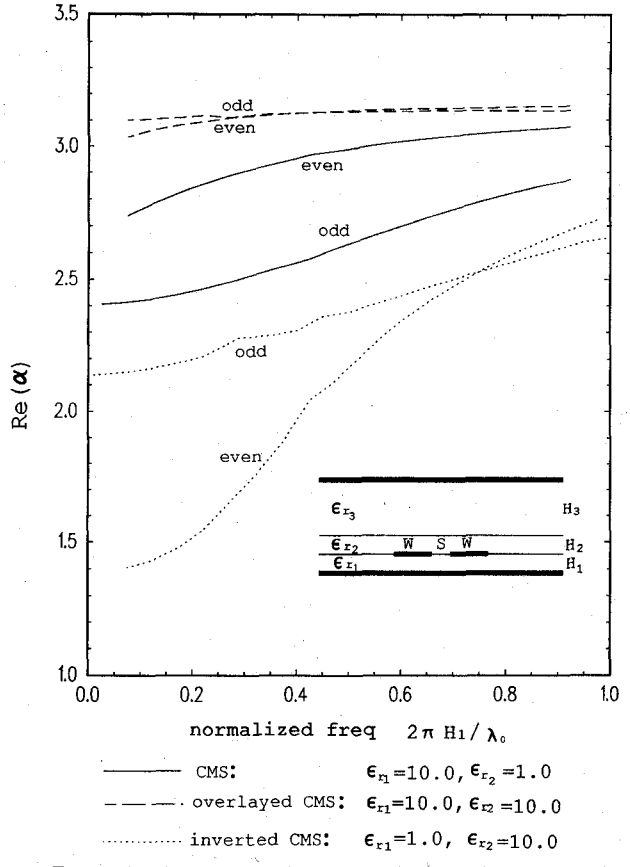


Fig. 7. Even and odd mode dispersion characteristics for three different types of coupled microstrip lines. $H_1 = H_2 = W, H_3 = 4H_1, S = 0.4$ W, $\epsilon_{r3} = 1.0$.

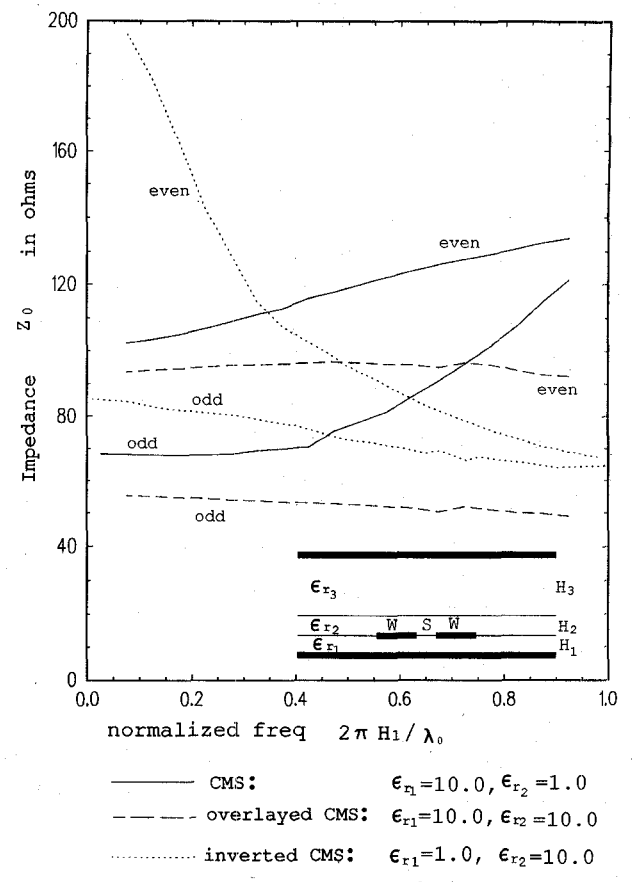


Fig. 8. Characteristic impedance defined by $P/I^2$ versus frequency for three types of CMS. $H_1 = H_2 = W, H_3 = 4H_1, S = 0.4$ W, $\epsilon_{r3} = 1.0$.

evanescent PPM's are used in the slot, below the strip and above the strip, respectively.

The result for the characteristic impedance $Z_0$ which is defined as $P/|I|^2/2$ is given in Fig. 8, where $I$ is the longitudinal current and $P$ is the total power over the cross-section. The general shape for the characteristic impedance based on the WH/GSMT agrees with that given in [18] but the values are higher than [18]. The characteristic impedance is more susceptible to numerical inaccuracies than the phase constant. This is analogous to the situation of the numerical computation of eigenvalues and eigenfunctions.

### *D. Antipodal Finline*

The antipodal finline depicted in Fig. 9 is chosen as an example to demonstrate the versatility of the WH/GSMT. The same parameters as in [19] are used in order to make a comparison. The normalized wavelength $\lambda_g/\lambda_0$ (= $1/Re[\alpha]$) and the characteristic impedance $Z_0$ versus the overlapped or separation length $s$ of two fins of the antipodal finline are given in Fig. 10. When the fins are overlapped, as depicted in Fig. 9(a), it behaves like a parallel plate waveguide with most of the fields concentrated in the overlapped region. The antipodal finline without overlapping, as depicted in Fig. 9(b), is similar to a unilateral finline, and it also resembles a partially filled waveguide as the two fins recede to the side walls.

For the overlapping case, the results for both $\lambda_g/\lambda_0$ and $Z_0$ agree well with [19]. For the nonoverlapping case, the

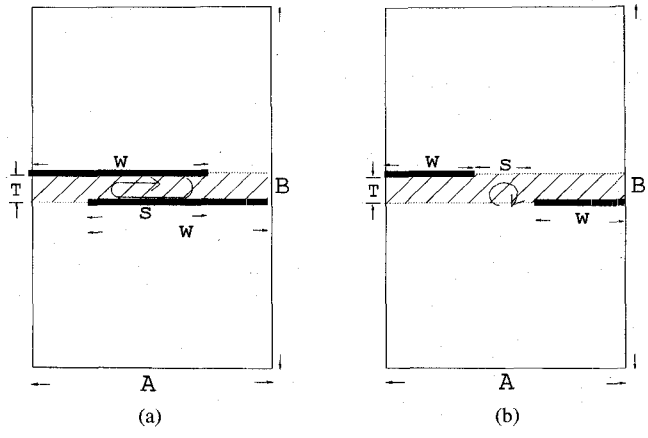


Fig. 9. Parameters used to describe (a) overlapped and (b) nonoverlapped antipodal finline geometries. $A = 2.845$ mm, $B = 5.69$ mm, $T = 0.127$ mm, $\epsilon_r = 2.22$.

agreement is reasonable for both $\lambda_g/\lambda_0$ and $Z_0$ when the operating frequency is 40 GHz. But for the other frequency, namely for 27 GHz, which is close to the $TE_{10}$ cut-off frequency 26.35 GHz for the rectangular waveguide (WG-22) enclosure, the result is quite different from that in [19] for both $\lambda_g/\lambda_0$ and $Z_0$. The impedance curves shown in Fig. 10(b) are obtained from the expression $V^2/P$. The integration path for computing the voltage $V$ for the overlapping case is a vertical path connecting the centers of the overlapped sections of the fins, whereas, it is a straight line between the edges of two

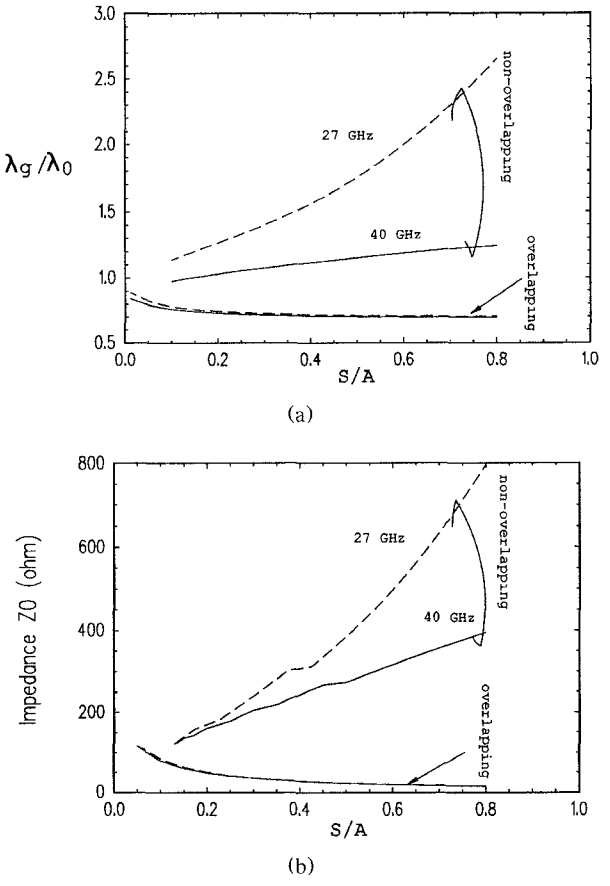


Fig. 10. (a) Normalized wavelength $\lambda_g/\lambda_0$ and (b) characteristic impedance $Z_0$ of the antipodal finline.

fins for the nonoverlapping case. Actually, the nonoverlapping case is not favorable for the WH/GSMT when the aspect ratio S/B (= 0.5 S/A) is too small since many evanescent PPM's have to be included. This is why there is a gap between the overlapping and nonoverlapping curves when S/A is small. However, when S/A is around 0.3 to 0.6, the results based on the WH/GSMT should be quite reliable, whereas, the spectral domain approach, used in [19], may require a large number of basis functions. Without further data from measurements or from other numerical methods, it is difficult to state which result is more accurate.

## V. Conclusions

A novel approach, based on a hybrid procedure referred to as the WH/GSMT, is developed to solve multilayered planar transmission line problems. It is a rigorous, full-wave analysis method. First, the scattering of an obliquely incident PPM by the edge of a PEC half plane embedded in a multilayered isotropic dielectric substrate within a PEC parallel plate region is analyzed via the WH technique. This solution is then incorporated in the formulation of the GSMT to find the propagation constants and characteristic impedances of a variety of planar transmission lines. The lateral power leakage is taken into account rigorously in the WH/GSMT. Numerical results including the cases for the microstrip line, conductor-backed slotline, coupled microstrip lines, and the antipodal finline are shown and compared with available references found in the literature to assess the accuracy of the WH/GSMT.

Compared with the widely used spectral domain approach (SDA), the WH/GSMT furnishes a different physical insight, is suited for planar transmission line configurations with relatively wide lateral dimensions, and requires similar amounts of CPU time and memory storage space if the ratio between the height and width of the parallel waveguide regions is not too large, but requires a more involved analysis. The versatility of the WH/GSMT is relatively limited because the complexity of the transverse resonance relations will increase rapidly as the transmission line configurations become more complicated. However, when the distance between the edges of the various PEC strips (or half planes) on the same dielectric interface is relatively large, the WH/GSMT may be more efficient than the SDA. In fact, as the lateral dimensions of the transmission lines become larger, the WH/GSMT becomes more efficient because a fewer number of evanescent modes are needed. On the other hand, the SDA becomes inefficient due to the large number of basis functions needed to obtain an accurate solution. One example where this point is demonstrated, is in the analysis of a conductor-backed coplanar waveguide (CBCPW) with finite extent lateral ground planes [20]–[23]. A detailed WH/GSMT based study of a CBCPW with single/double layered substrates and with finite/infinite lateral ground planes will be described in a separate paper. Generally, the WH/GSMT can be viewed as a more efficient version of the spatial mode-matching method and a complementary approach to the SDA. Note that in the WH/GSMT, the scattering matrix is obtained analytically, whereas, in the spatial mode matching method, this matrix is obtained numerically.

## VI. Appendix: Factorization of $Q_e(\lambda)$ and $Q_h(\lambda)$

As defined in (30) and (32),

$$Q_e(\lambda) = \frac{D_{2e}(\lambda)D_{3e}(\lambda)}{k_0 D_{1e}(\lambda)}, \tag{62}$$

and

$$Q_h(\lambda) = \frac{k_0 D_{2h}(\lambda)D_{3h}(\lambda)}{D_{1h}(\lambda)}. \tag{63}$$

There is more than one way to factorize $Q_e$ and $Q_h$ such that

$$Q_e(\lambda) = Q_{e_-}(\lambda)Q_{e_-}(\lambda) \tag{64}$$

and

$$Q_h(\lambda) = Q_{h_+}(\lambda)Q_{h_-}(\lambda). \tag{65}$$

where $Q_{e_{+(-)}}(\lambda)$ and $Q_{h_{+(-)}}(\lambda)$ are regular and free of zeros in the upper (lower) half $\lambda$ plane.

We also require

$$Q_{e_+}(-\lambda) = Q_{e_-}(\lambda) \tag{66}$$

and

$$Q_{h_+}(-\lambda) = Q_{h_-}(\lambda). \tag{67}$$

It is known that when $m$ is large [24],

$$\lambda_{1e_m} \sim -j\frac{(m-1)\pi}{k_0 A}, \quad \lambda_{2e_m} \sim -j\frac{(m-1)\pi}{k_0 D},$$
$$\lambda_{3e_m} \sim -j\frac{(m-1)\pi}{k_0 B}$$
$$\lambda_{1h_m} \sim -j\frac{m\pi}{k_0 A}, \quad \lambda_{2h_m} \sim -j\frac{m\pi}{k_0 D},$$
$$\lambda_{3h_m} \sim -j\frac{m\pi}{k_0 B}. \tag{68}$$

Based on the asymptotic behavior of these roots, a fast converging factorization for $Q_e$ [25] is given as follows.

$$Q_{e_+}(\lambda) = [Q_e(\lambda=0)]^{1/2} e^{\chi(\lambda)} \frac{\left(1-\frac{\lambda}{\lambda_{2e_1}}\right)\left(1-\frac{\lambda}{\lambda_{3e_1}}\right)}{\left(1-\frac{\lambda}{\lambda_{1e_1}}\right)} \cdot \frac{\mathcal{P}_{2e}(\lambda)\mathcal{P}_{3e}(\lambda)}{\mathcal{P}_{1e}(\lambda)} g(\lambda) \tag{69}$$

where

$$\chi(\lambda) = j\frac{\lambda k_0}{\pi}[D\ln(A/D) + B\ln(A/B)] \tag{70}$$

$$g(\lambda) = \frac{\Gamma(1-j\lambda k_0 A/\pi)}{\Gamma(1-j\lambda k_0 B/\pi)\Gamma(1-j\lambda k_0 D/\pi)}, \tag{71}$$

$\Gamma$ is the Gamma function and

$$\mathcal{P}_{1e}(\lambda) = \frac{\prod_{n=1}^{\infty}(1-\lambda/\lambda_{1e_{n+1}})}{\prod_{n=1}^{\infty}(1-j\lambda k_0 A/n\pi)}$$
$$\mathcal{P}_{2e}(\lambda) = \frac{\prod_{n=1}^{\infty}(1-\lambda/\lambda_{2e_{n+1}})}{\prod_{n=1}^{\infty}(1-j\lambda k_0 D/n\pi)}$$
$$\mathcal{P}_{3e}(\lambda) = \frac{\prod_{n=1}^{\infty}(1-\lambda/\lambda_{3e_{n+1}})}{\prod_{n=1}^{\infty}(1-j\lambda k_0 B/n\pi)} \tag{72}$$

Similarly,

$$Q_{h_+}(\lambda) = [Q_h(\lambda=0)]^{1/2} e^{\chi(\lambda)} \frac{\mathcal{P}_{2h}(\lambda)\mathcal{P}_{3h}(\lambda)}{\mathcal{P}_{1h}(\lambda)} g(\lambda) \tag{73}$$

where

$$\mathcal{P}_{1h}(\lambda) = \frac{\prod_{n=1}^{\infty}(1-\lambda/\lambda_{1h_n})}{\prod_{n=1}^{\infty}(1-j\lambda k_0 A/n\pi)}$$
$$\mathcal{P}_{2h}(\lambda) = \frac{\prod_{n=1}^{\infty}(1-\lambda/\lambda_{2h_n})}{\prod_{n=1}^{\infty}(1-j\lambda k_0 D/n\pi)}$$
$$\mathcal{P}_{3h}(\lambda) = \frac{\prod_{n=1}^{\infty}(1-\lambda/\lambda_{3h_n})}{\prod_{n=1}^{\infty}(1-j\lambda k_0 B/n\pi)}. \tag{74}$$

Since the variables $\alpha$ and $\lambda$ always appear in the form $\alpha^2+\lambda^2$ in $\overline{\overline{P}}_e$ and $\overline{\overline{P}}_h$, they can be treated as a single variable $\gamma = \alpha^2+\lambda^2$ when the zeros of $D_{ip}$ are searched. Once $\gamma_{ip_n}$ is determined, $\alpha^2$ can be subtracted from $\gamma_{ip_n}^2$ to get $\lambda_{ip_n}^2$. Thus, there is no need to search for $\lambda_{ip_n}$ again when $\alpha$ changes.

## REFERENCES


[1] L.-M. Chou, R. G. Rojas, and P. H. Pathak, "A WH/GSMT based full-wave analysis of multilayered printed transmission lines," *1992 IEEE APS/URSI Int.. Symp.*, July 1992.

[2] —, "A WH/GSMT based full-wave analysis of the power leakage from conductor-backed coplanar waveguide," *1992 IEEE MTT Int. Microwave Symp.*, June 1992.

[3] T. Itoh, Ed., *Numerical Techniques for Microwave and Millimeter-Wave Passive Structures.* New York: Wiley Interscience, 1989.

[4] R. Mittra and S. W. Lee, *Analytical Techniques in the Theory of Guided Waves.* New York: Macmillan, 1971.

[5] B. Noble, *Methods Based on the Wiener-Hopf Technique.* New York: Pergamon, 1958.

[6] K. S. Lee, "Microstrip line leaky wave antenna," Ph.D. dissertation, Polytechnic Univ., New York, June 1986.

[7] A. A. Oliner, "Leakage from higher order modes of microstrip line with application to antennas," *Radio Science*, vol. 22, no. 6, pp. 907–912, Nov. 1987.

[8] D. C. Chang and E. F. Kuester, "Total and partial reflection from the end of a parallel-plate waveguide with an extended dielectric slab," *Radio Science*, vol. 16, no. 1, pp. 1–13, Jan./Feb. 1981.

[9] T. Itoh, Ed., *Planar Transmission Line Structures.* New York: IEEE Press, 1987.

[10] N. K. Das and D. M. Pozar, "A generalized spectral-domain Green's function for multilayer dielectric substrates with application to multilayer transmission lines," *IEEE Trans. Microwave Theory Tech.*, vol. MTT-35, pp. 326–335, Mar. 1987.

[11] —, "Full-wave spectral-domain computation of material, radiation, and guided wave losses in infinite multilayered printed transmission lines," *IEEE Trans. Microwave Theory Tech.*, vol. MTT-39, pp. 54–63, Jan. 1991.

[12] J. A. Kong, *Electromagnetic Wave Theory.* New York: John Wiley & Sons, Inc., 1986.

[13] T. Itoh, "Spectral domain immitance approach for dispersion characteristics of generalized printed transmission lines," *IEEE Trans. Microwave Theory Tech.*, vol. MTT-28, no. 7, pp. 733–736, July 1980.

[14] Y.-C. Shih, T. Itoh, and L. Q. Bui, "Computer-aided design of millimeter-wave E-plane filters," *IEEE Trans. Microwave Theory Tech.*, vol. MTT-31, no. 2. pp. 135–142, Feb. 1983.

[15] S. T. Peng and A. A. Oliner, "Guidance and leakage properties of a class of open dielectric waveguides: part I—mathematical formulations," *IEEE Trans. Microwave Theory Tech .*, vol. MTT-29, no. 9, pp. 843–854, Sept. 1981.

[16] H. Ermert, "Guided modes and radiation characteristics of covered microstrip lines," *AEU*, vol. 30, pp. 65–70, 1976.

[17] H. Ermert, "Guiding and radiation characteristics of planar waveguides," *Microwaves, Optics and Acoustics* , vol. 3, no. 2, pp. 59–62, Mar. 1979.

[18] L. Su, T. Itoh, and J. Rivera, "Design of an overlay directional coupler by a full-wave analysis," *IEEE Trans. Microwave Theory Tech.*, vol. MTT-31, no. 12, pp. 1017–1022, Dec. 1983.

[19] D. Mirshekar-Syahkal and J. Brian Davies, "An accurate, unified solution to various fin-line structures, of phase constant, characteristic impedance, and attenuation," *IEEE Trans. Microwave Theory Tech.*, vol. MTT-30, no. 11, pp. 1854–1861, Nov. 1982.

[20] H. Shigesawa, M. Tsuji, and A. A. Oliner, "Conductor backed slotline and coplanar waveguide: Dangers and full-wave analysis," *IEEE MTT-S Int. Microwave Symp. Dig.*, 1988, pp. 199–202.

[21] R. W. Jackson, "Mode conversion as discontinuities in finite-width conductor-backed coplanar waveguide," *IEEE Trans. Microwave Theory Tech.*, vol. MTT-37, no. 10, pp. 1582–1589, Oct. 1989.

[22] M. Riaziat, R. Majidi-Ahy, and I-J. Feng, "Propagation modes and dispersion characteristics of coplanar waveguides," *IEEE Trans. Microwave Theory Tech.*, vol. MTT-38, pp. 245-251, Mar. 1990.
[23] G. Ghione and C. U. Naldi, "Coplanar waveguides for MMIC applications: effect of upper shielding, conductor backing, finite-extent ground planes, and line-to-line coupling," *IEEE Trans. Microwave Theory Tech.*, vol. MTT-35, pp. 260–267, Mar. 1987.
[24] R. Mittra, Ed., *Computer Techniques for Electromagnetics.* Washington D.C.: Hemisphere Publishing Corp., ch. 6, 1987.
[25] R. Janaswamy, "Wiener-Hopf analysis of the asymmetric slotline," *Radio Science*, vol. 25, no. 5, pp. 699–706, Sept./Oct. 1990.

**Ling-Miao Chou** was born in Taipei, Taiwan, in 1964. She received the B.S.E.E. degree from the National Taiwan University, Taipei, Taiwan, in 1986, and the M.S. and Ph.D. degrees in electrical engineering from The Ohio State University, Columbus, Ohio, in 1988 and 1992, respectively.

In 1993, she joined the Solid State Microwave Technology Department at the Electronics Research and Service Organization, in the Industrial Technology Research Institute, Hsinchu, Taiwan, where she works as a mi- crowave circuit design engineer. She is responsible for designing RF and microwave circuits for consumer electronics products.

**Roberto G. Rojas** (S'80–M'85–SM'90) received the B.S.E.E. degree from New Mexico State University, in 1979, and the M.S. and Ph.D. degrees in electrical engineering from The Ohio State University, in 1981 and 1985, respectively.

During the summer of 1979, he worked with Rockwell International in Albuquerque, New Mexico. He has been with The Ohio State University ElectroScience Laboratory since 1979, first as a graduate student and starting in 1985 as a full-time researcher. He spent three months at the Jet Propulsion Laboratory as a Summer Faculty Fellow in 1993. His current research interests are in electromagnetic scattering, radiation and modeling, high-frequency techniques, and development of numerical and analytical techniques for the analysis of MMIC. Dr. Rojas has won the 1988 R.W.P. King Prize Paper Award and the 1990 Browder J. Thompson Memorial Prize Award, both given by IEEE, and the 1989 and 1993 Lumley Research Awards, given by the College of Engineering at The Ohio State University.

Dr. Rojas has served as Chairman, Vice-Chairman and Secretary/Treasurer of the Columbus, OH chapter of the IEEE Antennas and Propagation and Microwave Theory and Techniques Societies. He is an elected mem ber of U.S. Commission B of URSI.

**Prabhakar H. Pathak**, for a photograph and biography, see page 702 of April 1993 issue of this TRANSACTIONS.